


# Passive Radar STAP Detection and DoA Estimation Under Antenna Calibration Errors

GIOVANNI PAOLO BLASONE , Student Member, IEEE

FABIOLA COLONE , Senior Member, IEEE

PIERFRANCESCO LOMBARDO , Senior Member, IEEE  
Sapienza University of Rome, Rome, Italy

PHILIPP WOJACZEK , Member, IEEE

DIEGO CRISTALLINI , Member, IEEE

Fraunhofer Institute for High Frequency Physics and Radar Techniques,  
Wachtberg, Germany

**This article addresses the problem of clutter cancelation for slowly moving target detection and localization in multichannel passive radar onboard mobile platforms. A post-Doppler space-time adaptive processing (STAP) approach is exploited in the case of an angle-dependent imbalance affecting the receiving channels. While the clutter suppression capability is ensured by the adaptivity of space-time filtering, different solutions are compared, aimed at recovering the detection performance losses associated with channel calibration errors. A space-time generalized-likelihood ratio test (GLRT) scheme is considered, where the steering vector is not specified in the spatial domain, resulting in a noncoherent integration of target echoes across the receiving channels. This is compared with a fully coherent GLRT scheme where echoes from the stationary scene are exploited for the proper calibration of spatial steering vector mismatch. The first scheme proves to be a simple solution for target detection in the passive radar case, offering comparable clutter cancelation capability. The**

Manuscript received August 20, 2020; revised December 17, 2020; released for publication February 7, 2021. Date of publication February 25, 2021; date of current version October 11, 2021.

DOI. No. 10.1109/TAES.2021.3061803

Refereeing of this contribution was handled by K. S. Kulpa.

This work was supported by the Italian Ministry of University and Research Project Safety and Security Systems for Sea Environment SCN\_00393.

Authors' addresses: Giovanni Paolo Blasone, Fabiola Colone, and Pierfrancesco Lombardo are with the Department of Information Engineering, Electronics, and Telecommunications, Sapienza University of Rome, 00184 Rome, Italy, E-mail: (giovannipaolo.blasone@uniroma1.it; fabiola.colone@uniroma1.it; pierfrancesco.lombardo@uniroma1.it); Philipp Wojaczek and Diego Cristallini are with the Fraunhofer Institute for High Frequency Physics and Radar Techniques, 53343 Wachtberg, Germany, E-mail: (philipp.wojaczek@fhr.fraunhofer.de; diego.cristallini@fhr.fraunhofer.de). (*Corresponding author: Giovanni Paolo Blasone.*)

This work is licensed under a Creative Commons Attribution 4.0 License. For more information, see <https://creativecommons.org/licenses/by/4.0/>

second scheme, at the expense of an additional stage, offers slightly better detection performance and preserves target direction-of-arrival (DoA) estimation capability. Finally, the STAP scheme is employed for the maximum-likelihood estimation of target DoA, evaluating the role of the steering vector calibration against the negative impact of channel imbalance. The effectiveness of the proposed approaches is tested against both simulated and experimental data from a DVB-T-based mobile passive radar.

## I. INTRODUCTION

Over the past few years, renewed and increasing attention has been devoted by the scientific community to the passive radar technology. Recent advances in this field have opened new perspectives and innovative areas of research [1]–[3]. Among them, one of the most interesting and challenging is the use of passive radar onboard airborne or ground moving platforms.

The application to mobile platforms allows to extend the functionalities of passive radar to applications, such as synthetic aperture radar (SAR) imaging [4]–[7] or ground moving target indication (GMTI) [8]–[19], thus yielding the well-known advantages of this kind of sensors to airborne class systems.

The strategic advantages of a mobile passive radar are paid by the motion-induced Doppler distortions of the received signals. The reference signal should be collected and reconstructed regardless of the platform motion [20], [21]. Moreover, the Doppler-spread clutter returns from the stationary scene, typical of moving radar, can hinder the detection of moving targets with a small radial velocity component. This effect tends to be even more stressed at the very/ultra high frequency (VHF/UHF) bands of the most widely used illuminators of opportunity due to the typical broad antenna beams available. The detection of slow-moving targets requires a proper suppression of clutter echoes, which can be achieved by exploiting systems with multiple receiving channels, enabling space-time processing.

The first attempts of providing GMTI capability to mobile passive radar exploited the displaced phase center antenna (DPCA) approach [8]–[13]. DPCA performs a nonadaptive subtraction of properly delayed radar echoes collected by two along-track displaced receiving channels [27]. Thus, it requires a simple architecture and limited computational load, which make it attractive for the passive radar application.

The first proof of concept of DPCA in mobile passive radar is given in [8] and [9] for the experimental data from an airborne FM-based passive radar and against the simulated digital video broadcasting - terrestrial (DVB-T) data.

In [10], an effective processing scheme is proposed based on a flexible DPCA approach in conjunction with a reciprocal filtering strategy for the range compression stage [25], [26], which removes the performance limitations deriving from the uncontrolled temporal variability of the exploited opportunity waveform. Its effectiveness is proved for a DVB-T-based passive radar against both simulated and experimental data.

However, significant limitations to the DPCA performance may come from the amplitude and/or phase imbalance possibly affecting the receiving channels [11], [12]. Such imbalance can be in general function of the angle of arrival due to several factors: dissimilarities between receiving antennas, mutual coupling effects, and interaction with near-field obstacles.

Channel imbalance is a well-known issue in active radar. Its role has been largely analyzed in the literature in the context of array beamforming and space-time processing [27], [28]. For specific applications and operational conditions, the accurate factory or in-field calibration might be not feasible or not sufficient. Methods for array self-calibration have been studied [29]–[31] as well as space-time techniques in the presence of steering vector mismatch [32]. Strategies for adaptive digital channel calibration based on the received data have been developed in [33] and [34] for the case of SAR-GMTI.

In the passive radar case, several aspects brought in by the passive bistatic operation make the channel imbalance a critical problem, limiting the applicability of the conventional calibration strategies and severely compromising the system performance, especially in the case of GMTI applications.

Due to the wavelength of the most exploited illuminators of opportunity, the typical antennas available are characterized by broad beams and relatively high sidelobes. The low directivity of receiving antennas is paired with a bistatic illumination from broadcast transmitters, which do not focus the signal energy only in the direction of interest. This results in nonnegligible clutter echoes arriving from a very wide angular sector as well as in a strong direct-path interference. Such contributions are simultaneously received, forming a wide clutter Doppler bandwidth, and are very likely affected by a diverse amplitude and phase response across the receiving channels. In addition, the commercial-off-the-shelf components, commonly used in the low-cost passive radar hardware, and the long wavelength of typical opportunity signals may pose some limitations to the accuracy (or feasibility) of preliminary system calibration. As a result, the receiving channels may be easily affected by nonnegligible residual angle-dependent imbalance, as also verified on the experimental data in [13]. The above critical aspects must be tackled to ensure effective clutter cancelation and moving target detection and localization capability while possibly preserving the low-cost paradigm, typical of passive radar.

On the other hand, the typical long integration times of passive radar provide a fine Doppler frequency resolution, which can be conveniently exploited. In [13], effective ad-hoc solutions are developed for channel calibration in passive radar DPCA. The proposed strategies take the advantage of the clutter angle-Doppler dependence for the estimation of angle-dependent imbalances. The accurate calibration of the received data proved to be largely required to preserve clutter suppression capability.

The intrinsic limitations of DPCA and its reliance on an adaptive calibration stage for the compensation of localized

errors suggest moving in the direction of a space-time adaptive processing (STAP) approach [14]. At the expense of a higher computational load, STAP has more flexibility and adaptation capability, thanks to a higher number of adaptive degrees of freedom. The use of STAP for clutter rejection in passive radar was first considered in [15] and [16]. The preliminary experimental results of STAP in a DVB-T-based mobile passive radar are presented in [17]. In [18], sparse Bayesian learning is employed for the accurate estimation of clutter covariance matrix based on few secondary samples. In [19], a 3-D model is proposed to integrate clutter modeling and waveform impact in passive STAP. Further applications of STAP in the passive radar are considered: in [22], for improved target detection exploiting spatial diversity with orthogonal frequency division multiplexing (OFDM) waveforms; in [23], for direct signal interference suppression; and in [24], for clutter rejection in airborne bistatic inverse-SAR imaging.

In this article, we propose a STAP scheme for mobile passive radar and analyze its effectiveness in terms of clutter cancelation and moving target detection and localization, in the case of an unknown angle-dependent imbalance affecting the receiving channels. The set of adopted methodologies takes the advantage of the characteristics of the passive radar scenario.

First, we point out the fundamental role of a post-Doppler STAP approach in preserving clutter cancelation capability, also in the presence of channel calibration errors, identifying it as particularly suitable for mobile passive radar. It takes the advantage of the long integration time and the resulting fine Doppler resolution to considerably reduce the size of the adaptive problem and intrinsically compensate for the angle-dependent channel errors by operating on a clutter subspace accounting for a limited angular sector.

Therefore, we propose two detection schemes aimed at mitigating the effects of the channel imbalance on the target signal, whose direction-of-arrival (DoA) and experienced imbalance may differ from those of the surrounding clutter, possibly affecting the detection and localization performance, despite the effective clutter suppression.

The first scheme consists of a partially noncoherent generalized-likelihood ratio test (GLRT), which performs a noncoherent integration of the target signal across the receiving channels, to cope with losses due to spatial steering vector mismatch. Entirely excluding the presence of a calibration stage, it provides a simple solution for target detection in systems featuring few receiving channels. The second scheme consists of a fully coherent GLRT, where the echoes from the stationary scene are exploited to estimate the channel errors in the desired target search direction and calibrate the spatial steering vector, making use of the known relationship between the angle of arrival and Doppler frequency of stationary scatterers. At the expense of an additional calibration stage, this solution provides better detection performance and preserves target DoA estimation capability.

Finally, we address the target angular localization problem. The limited number and low directivity of receiving

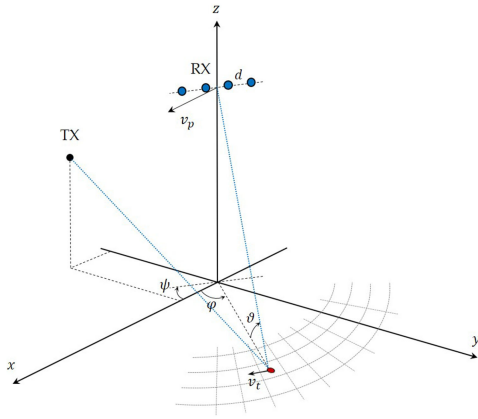


Fig. 1. System geometry for a multichannel mobile passive radar exploiting a stationary illuminator of opportunity.

antennas, due to the typically exploited wavelengths, make the accurate estimation of the target DoA a critical task. Such capability requires the availability of multiple spatial degrees of freedom, which must be properly exploited both for space-time clutter filtering and for target DoA estimation, and it can be severely compromised by the presence of channel imbalance. To this purpose, the proposed STAP scheme is adopted for a maximum-likelihood (ML) DoA estimation, assessing the key role of the steering vector calibration in mitigating the negative impact of the unknown channel errors.

Moving target detection and localization performances of the proposed solutions are analyzed and compared against a simulated clutter scenario. Moreover, some results are shown against the experimental data collected by a DVB-T-based multichannel passive radar mounted on a ground moving platform. The obtained results clearly demonstrate the effectiveness of the proposed strategies.

The rest of the article is organized as follows. In Section II, the signal model and the considered processing scheme for passive radar STAP are described. The impact of channel calibration errors on the moving target detection performance is addressed in Section III. In Section IV, two schemes are proposed for the target detection under channel imbalance conditions and their performances are analyzed against a simulated clutter scenario in Section V. Section VI is concerned with the target DoA estimation problem and the accuracy of an ML estimator is analyzed against the simulated data, studying the role of steering vector calibration. In Section VII, the effectiveness of the proposed strategies is validated against a set of experimental data. Finally, Section VIII concludes this article.

## II. STAP SCHEME FOR PASSIVE RADAR

Let us consider an  $N$  channel passive radar receiver mounted on a moving platform and exploiting a stationary transmitter as an illuminator of opportunity (see Fig. 1). The platform moves at a constant velocity  $v_p$  on a straightline trajectory, assumed without the loss of generality along the

$x$ -axis. Angles  $\varphi$  and  $\vartheta$  indicate, respectively, the azimuth and depression angle of the receiver to scatterer line of sight.

By recalling the signal model adopted in [10], for a linear array of elements equally spaced by  $d$  in a side-looking configuration (crab angle  $\psi = 0$ ), the discrete-time baseband signal received at the  $i$ th antenna from a moving target at angles  $(\varphi_0, \vartheta_0)$  and bistatic range  $R_b$  can be expressed as

$$r_0^{(i)} [l] = G_i(\varphi_0, \vartheta_0) A_0 \sum_n s_n [l - nL - l_{\tau_0}] \times e^{j2\pi f_D nT} e^{-j2\pi i \frac{d}{\lambda} \cos \varphi_0 \cos \vartheta_0} \quad (1)$$

where

- $l$  is the time index, representing the  $l$ th sample of discrete-time signals, sampled at a frequency  $f_s$ .
- The transmitted signal is partitioned in batches of duration  $T$  and  $s_n[l]$  denotes the  $n$ th batch, which is nonzero in the interval  $[0, L - 1]$ , where  $L = Tf_s$  is the number of samples in each batch; notice that the Doppler-induced phase term within each batch has been neglected.
- $l_{\tau_0} = f_s R_b/c$  is the bistatic propagation delay, assumed constant during the observation time.
- $A_0$  is the target complex amplitude and  $G_i(\varphi_0, \vartheta_0)$  is the complex gain of the  $i$ th channel; the latter represents the overall receiver chains, including the antenna pattern, and encodes possible imbalance between the channels.
- $f_D$  is the bistatic Doppler frequency, which can be expressed as the sum of two contributions as follows:

$$f_D = \frac{v_p}{\lambda} \cos \varphi_0 \cos \vartheta_0 - \frac{v_b}{\lambda} \quad (2)$$

the first is related to the platform motion and the receiver to scatterer geometry, and the second is due to the target intrinsic bistatic radial velocity  $v_b$ ;  $\lambda$  denotes the signal carrier wavelength.

The signal representing the clutter contribution before range compression can be expressed as the superposition of echoes from a distribution of stationary scatterers ( $v_b = 0$ ) at different bistatic ranges  $R_q$  ( $q = 1, \dots, N_R$ ) and different angles  $\varphi$

$$r_C^{(i)} [l] = \sum_{q=1}^{N_R} \int_{\varphi} G_i(\varphi, \vartheta) A_q(\varphi) \sum_n s_n [l - nL - l_{\tau_q}] \times e^{j2\pi \frac{v_p}{\lambda} \cos \varphi \cos \vartheta nT} e^{-j2\pi i \frac{d}{\lambda} \cos \varphi \cos \vartheta} d\varphi \quad (3)$$

where  $A_q(\varphi)$  is the complex amplitude and  $\tau_q$  is the bistatic propagation delay of echo from clutter patch at angle  $\varphi$  and range  $R_q$ .

The adopted processing scheme for the application of STAP to the passive radar framework is sketched in Fig. 2. It is obtained by extending the DPCA scheme presented in [10] to the general case of an  $N$  channel receiver. The scheme is based on a batch processing architecture, which recreates the conventional fast-time/slow-time framework of a pulsed radar system operating at an equivalent pulse

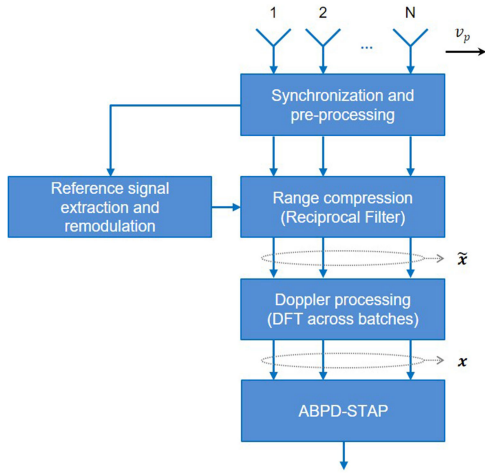


Fig. 2. Sketch of the processing scheme of a post-Doppler STAP approach for passive radar.

repetition frequency (PRF) given by the inverse of the batch duration ( $\text{PRF} = 1/T$ ). The range compression stage is performed for each batch by means of a reciprocal filter, which has the dual role of controlling the signal ambiguity function and removing the temporal variability of the employed opportunity waveform (see [10] for more details). For this purpose, a perfect reconstruction of the reference signal is supposed available by means of a decode/recode approach.

After the range compression stage, by collecting the samples associated with the range cell under test, from the  $N$  receiving channels and the  $M$  batches in the coherent processing interval (CPI), the  $(NM \times 1)$  space-time data vector  $\tilde{\mathbf{x}}$  is obtained. In the presence of a target with Doppler frequency  $f_D$ , DoA  $\phi$ , and complex amplitude  $\tilde{A}$ , the data vector can be written as  $\tilde{\mathbf{x}} = \tilde{A}\tilde{\mathbf{s}} + \tilde{\mathbf{d}}$ , where  $\tilde{\mathbf{d}}$  represents the disturbance (clutter plus noise) component, assumed Gaussian with space-time covariance matrix  $\tilde{\mathbf{Q}} = E\{\tilde{\mathbf{d}}\tilde{\mathbf{d}}^H\}$ . The space-time steering vector  $\tilde{\mathbf{s}}$  can be expressed as  $\tilde{\mathbf{s}}(f_D, \phi) = \mathbf{s}_t(f_D) \otimes \mathbf{s}_s(\phi)$ , where  $\mathbf{s}_t(f_D) = [1, e^{-j2\pi f_D T}, \dots, e^{-j2\pi f_D M T}]^H$  is the temporal steering vector and  $\mathbf{s}_s(\phi) = [1, e^{j2\pi d/\lambda \cos \phi}, \dots, e^{j2\pi Nd/\lambda \cos \phi}]^H$  is the spatial steering vector;  $\otimes$  denoting the Kronecker product and  $H$  is the Hermitian transpose. Notice that  $\phi$  denotes the angle between the antenna endfire and the receiver to scatterer line of sight ( $\cos \phi = \cos(\varphi - \psi) \cos \vartheta$ ).

As known, STAP adaptively combines the spatial and temporal samples of the signal in order to suppress clutter in the angle-Doppler domain and maximize the detection probability of potential moving targets [27]. It is based on the inversion of the space-time disturbance covariance matrix  $\tilde{\mathbf{Q}}$ , which is usually not available in practical applications and has to be estimated based on proper training data. In order to reduce the computational effort and the amount of training data required for an effective estimation of  $\tilde{\mathbf{Q}}$ , a number of reduced-order STAP approaches have been suggested, where adaptive processing is applied after a nonadaptive projection of data in a proper subspace [35].

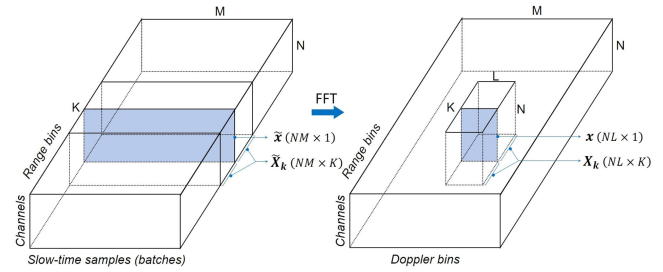


Fig. 3. Graphical illustration of the formation process of data vectors  $\tilde{\mathbf{x}}$ ,  $\mathbf{x}$ , and matrix  $\mathbf{X}_k$ , according to the ABPD approach. Notice that the fast Fourier transform operation is performed in the slow-time domain, represented by the signal batches.

The post-Doppler STAP approaches, where adaptation occurs on a subset of Doppler processed data, are particularly suitable for the passive radar case, characterized by relatively long integration times. In fact, sufficiently long CPIs ensure a proper decoupling of different clutter Doppler components. Specifically, we consider an adjacent-bin post-Doppler (ABPD) approach, which adaptively combines the  $N$  spatial samples from a subset of  $L$  adjacent Doppler bins centered at the cell under test.

Let  $\mathbf{T}$  be a transformation matrix, which consists, in this case, of  $L$  adjacent columns of a discrete Fourier transform matrix. The resulting vectors in the space-Doppler domain are given by  $\mathbf{x} = \mathbf{T}^H \tilde{\mathbf{x}}$  and  $\mathbf{s} = \mathbf{T}^H \tilde{\mathbf{s}} = \mathbf{s}_d \otimes \mathbf{s}_s(\phi)$  of size  $(NL \times 1)$ . The corresponding  $(NL \times NL)$  space-Doppler disturbance covariance matrix will be  $\mathbf{Q} = \mathbf{T}^H \tilde{\mathbf{Q}} \mathbf{T}$ .

Fig. 3 offers a graphical illustration of the formation process of the data vector and the related training data, according to the adopted ABPD approach.

The well-known space-time GLRT detector can be easily derived following the approach in [36] and applied after the ABPD transformation:

$$\frac{|s^H \hat{\mathbf{Q}}^{-1} \mathbf{x}|^2}{s^H \hat{\mathbf{Q}}^{-1} \mathbf{s} (1 + \mathbf{x}^H \hat{\mathbf{Q}}^{-1} \mathbf{x})} \geq \eta_1 \quad (4)$$

where matrix  $\mathbf{Q}$  is substituted by its ML estimate  $\hat{\mathbf{Q}} = \mathbf{X}_k \mathbf{X}_k^H$ , being  $\mathbf{X}_k = [\mathbf{x}_1, \dots, \mathbf{x}_K]$  a set of training data of size  $(NL \times K)$  from  $K$  adjacent range cells, assumed as statistically independent, identically distributed and target free. The detection threshold  $\eta_1$  is selected according to the desired value of false alarm probability (PFA), whose known analytical expression is

$$\text{PFA} = \left(\frac{1}{l}\right)^{K-NL+1} \quad (5)$$

where  $l = 1/(1 - \eta_1)$ .

STAP solution can handle a higher number of degrees of freedom, offering more flexibility and adaptation capability compared with the DPCA approach. On the one hand, it has a higher computational effort since it requires the estimation and inversion of a covariance matrix potentially for each range-Doppler bin. However, the ABPD approach limits the computational cost and the number of required training

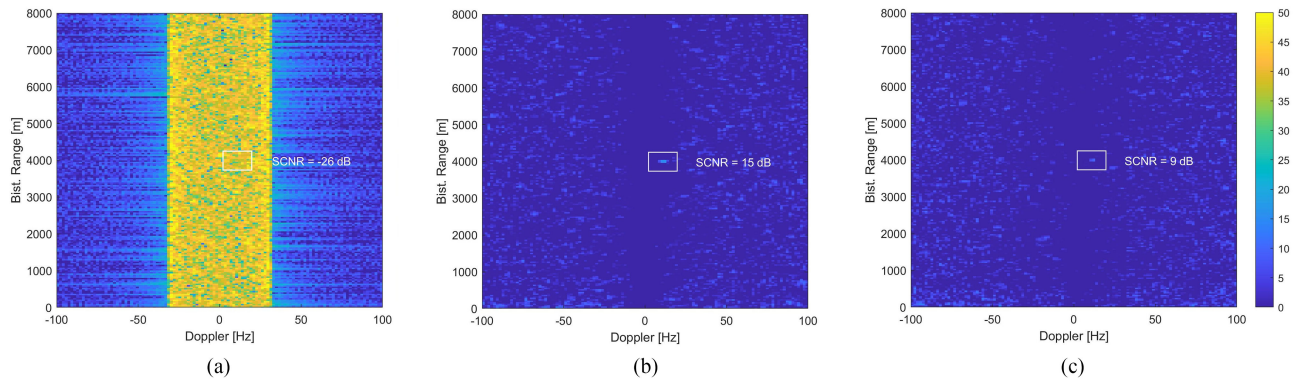


Fig. 4. Range-Doppler maps from simulated clutter scenario. (a) Single-channel RD map. (b) RD map after ABPD-STAP with perfectly balanced channels. (c) RD map after ABPD-STAP in the presence of channel imbalance.

data by significantly reducing the size of the covariance matrix. This also plays a key role in a real scenario, where the effectiveness of STAP would be subject to the potential nonhomogeneity of clutter, which might not offer a sufficient number of relevant training data for matrix estimation.

In order to analyze the effectiveness of the considered space-time processing scheme in a controlled environment, we test it against a simulated clutter scenario for a multi-channel moving passive radar.

We assume a ground moving receiver exploiting a stationary transmitter in a quasi-monostatic geometry. An 8k mode DVB-T signal sequence is generated as a reference signal. The details on the DVB-T signal parameters can be found in Table I of Section VII. Clutter returns are generated according to the model in (3) for a scene spanning  $N_R = 1000$  range cells. Amplitudes  $A_q(\varphi)$  associated with different clutter patches are assumed independent and identically distributed complex Gaussian variables, thus resulting in a homogeneous clutter scenario. We assume the availability of  $N = 3$  perfectly balanced receiving channels, arranged in the along-track direction, in a side-looking configuration. Omnidirectional antennas are considered within an angular sector  $\varphi = [0, \pi]$  (no backlobe contributions). Carrier frequency is set to 690 MHz, platform velocity  $v_p = 13$  m/s, and antenna element spacing  $d = \lambda/2$ . We consider a CPI length of 512 OFDM symbols, corresponding to approximately half a second ( $\sim 0.57$  s), and we assume the absence of internal clutter motion. Notice that the DVB-T elementary period ( $7/64 \mu\text{s}$ ) defines the fast-time sampling rate, while the batch duration, deliberately selected as equal to the OFDM symbol duration, defines the slow-time sampling rate (equivalent PRF  $\cong 893$  Hz).

The generated input signal includes clutter returns and thermal noise and is scaled so that the overall clutter contribution has an assigned power level of 20 dB above the noise level at the input of each channel. The echo from a moving target is also included with a bistatic range  $R_b = 4$  km, angle of arrival  $\phi_0 = 90^\circ$ , and bistatic radial velocity  $v_b = 5$  m/s. The target signal-to-noise ratio (SNR), defined as the ratio of target signal power level with respect to noise, at the input of each channel before range compression, is set to  $-43$  dB.

The range-Doppler map obtained from a single channel is reported in Fig. 4(a). As apparent, clutter returns appear across a Doppler extension of approximately  $\pm v_p/\lambda \cong \pm 30$  Hz, while the target signal-to-clutter plus noise ratio (SCNR) is  $-26$  dB. The target SCNR is measured by taking the power level at the target range-Doppler location, when the processing is fed with target echoes only, and disturbance power level estimated over a proper area surrounding target location, in the maps containing only clutter and noise.

Applying the ABPD-STAP scheme in Fig. 2, the resulting range-Doppler map at the output of the adaptive filter [numerator in (4)] is shown in Fig. 4(b). In particular,  $L = 3$  adjacent Doppler bins are used for a total on  $NL = 9$  degrees of freedom. The number  $L$  of Doppler bins is generally selected as small as possible, to reduce the computational complexity, but sufficient to guarantee good clutter cancellation capability. In our case, the value  $L = 3$  proved to be a suitable tradeoff between the required cost and effectiveness of the adaptive filter. The number of training data is set to  $K = 6NL = 54$ . This large sample support is selected in order to minimize the undesirable adaptivity losses. Notice that the range-Doppler maps are scaled to provide unitary processing gain for thermal noise, thus allowing a direct comparison of results. As expected, the clutter background is effectively canceled and the resulting target SCNR is 15 dB with an overall improvement of 41 dB.

### III. LIMITATIONS DUE TO CHANNEL CALIBRATION ERRORS

To analyze the effects of channel imbalance, we include in the simulation process the presence of a deterministic but unknown angle-dependent imbalance between the receiving channels. We denote by  $\Gamma_{ij}(\phi) = G_i(\phi)/G_j(\phi)$  the complex imbalance between channels  $i$  and  $j$ . Specifically, we assume a sinusoidal phase imbalance, as illustrated in Fig. 5, where channel 1 is arbitrarily taken as reference. Notice that the channel error is modeled as a function of the angle  $\phi$  between the array line and the receiver to scatterer line of sight.

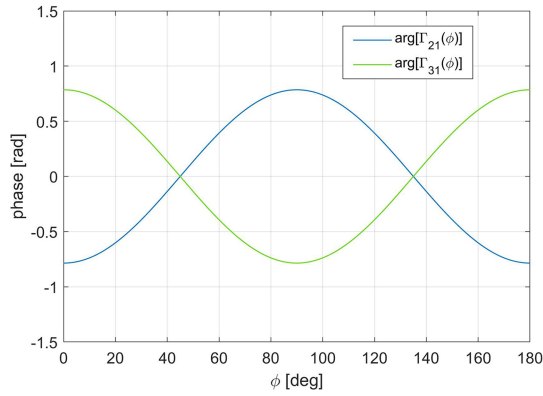


Fig. 5. Simulated phase imbalance between the receiving channels as a function of the angle of arrival.

It is also worth noting that the level of the simulated phase imbalance in Fig. 5 is of the same order of magnitude of the imbalance experienced on the experimental data in [13].

The range-Doppler map resulting at the output of the STAP scheme in the presence of channel imbalance is reported in Fig. 4(c). ABPD approach with  $L = 3$  and  $K = 54$  is again applied. As expected, the adaptation capability of the STAP filter allows to intrinsically compensate for the angle-dependent channel errors and keeps providing an effective cancelation of clutter echoes. In this sense, the use of a post-Doppler approach plays a fundamental role. In fact, the known one-to-one relationship between the angle of arrival and Doppler frequency of stationary scatterers, as well as the fine Doppler resolution guaranteed by the long integration times of passive radar, allows the ABPD approach to operate on a clutter subspace accounting for a limited angular sector. This allows to significantly reduce the number of degrees of freedom of the adaptive filter by still being able to compensate for the angular variation of channel imbalance.

However, although STAP proves robust against channel imbalance for what concerns clutter suppression capability, the same cannot be said for the corresponding target steering vector used in the adaptive filter. In fact, the presence of unknown channel errors may cause a mismatch between the nominal spatial steering vector  $s_s(\phi)$  and the actual target vector affected by the channel imbalance, which can be modeled as  $\text{diag}\{[1, \Gamma_{21}(\phi), \dots, \Gamma_{N1}(\phi)]\} s_s(\phi)$ , by taking channel 1 as a reference without the loss of generality. This may result in target signal gain losses. In the case of Fig. 4(c), the final target SCNR is in fact limited to 9 dB.

Fig. 6 shows the target signal response in the angle-Doppler domain at the output of the optimum space-time filter without (a) and with (b) the effect of channel imbalance. Such result is evaluated in the absence of noise and known covariance matrix case and can be seen as the theoretical output SCNR achievable, normalized to its maximum, as a function of the target DoA and Doppler frequency. In both cases, we recognize the typical clutter ridge of a side-looking configuration but the presence of channel imbalance produces a slight deformation and an

enlargement of the clutter notch. Moreover, we notice a dispersion of the clutter energy in the angle-Doppler domain due to the angle-dependent imbalance. This results in losses also far from the clutter notch as an effect of the adaptive cancelation filter.

In order to evaluate the performance losses associated with the presence of channel imbalance in terms of target detection capability, a Monte Carlo analysis is performed, assuming the same simulated scenario and processing parameters adopted in the previous example. The space-time GLRT detector in (4) is considered with a desired PFA set to  $10^{-6}$ . A Swerling 0 target model is assumed.

In Fig. 7, the results are shown in terms of probability of detection (PD) as a function of target input SNR. Two targets are considered with bistatic velocity 7 m/s and 3 m/s at DoA  $\phi_0 = 90^\circ$ . They are representative of the target condition close and sufficiently far from the clutter notch. The dashed curves in the figure represent the detection performance achievable in the absence of channel imbalance, while the solid curves show the corresponding performance when receiving channels are affected by the imbalance in Fig. 5.

A significant loss can be observed, especially for a target velocity of 3 m/s, corresponding to a slow target close to the clutter notch. This indicates that the presence of channel mismatch may increase the clutter rank and produce an enlargement of clutter notch (as from [28]), thus raising the target minimum detectable velocity (MDV). This is also confirmed by looking at Fig. 8, where PD is evaluated as a function of target bistatic velocity for a fixed SNR of  $-45$  dB.

Notice that a decrease in PD performance is present also for higher velocity values. This is mostly caused by the mentioned dispersion of clutter energy in the angle-Doppler domain, which has to be canceled by the adaptive filter [see depressions in Fig. 6(b)].

#### IV. SOLUTIONS FOR TARGET DETECTION

We have shown how the presence of an unknown imbalance affecting the receiving channels can impact on moving target detection performance of a mobile passive radar. In particular, when adopting a STAP approach on a multichannel system, the mismatch of target steering vector, as well as the coefficients estimated for the cancelation of clutter, may result in undesirable gain loss or even partial suppression of target signal at the output of the adaptive filter.

It is worth noting that applying digital channel calibration techniques, such as those proposed in [13], to the received data is crucial to guarantee clutter cancelation in a nonadaptive approach, such as DPCA, while it is not strictly required in the STAP case. In fact, the adaptation capability of STAP can intrinsically compensate for localized channel errors, thus preserving clutter suppression capability. Moreover, in the case of angle-dependent channel errors, the target signal may experience a different imbalance compared with clutter contributions appearing at the same Doppler frequency since belonging to a different angular direction.

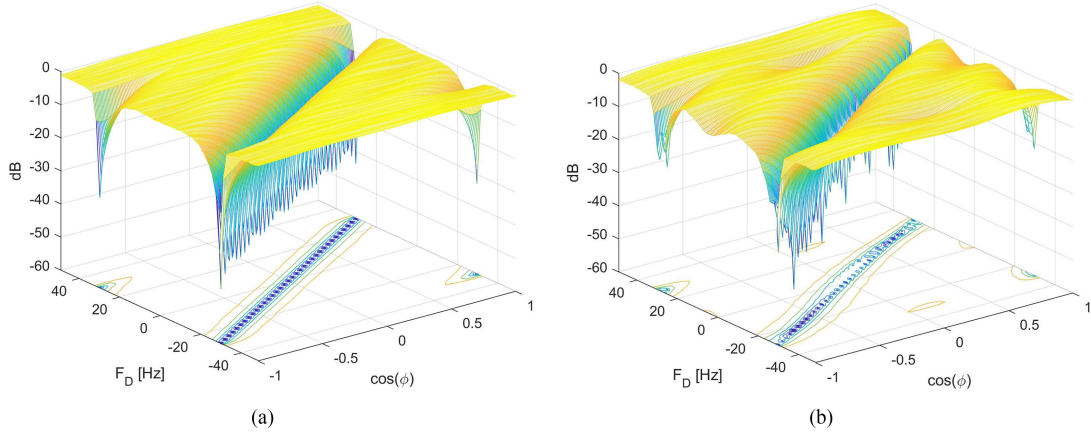


Fig. 6. Target signal response in the angle-Doppler domain at the output of the optimum space-time filter in the absence of noise and for the known covariance matrix. (a) With perfectly balanced channels. (b) In presence of channel imbalance.

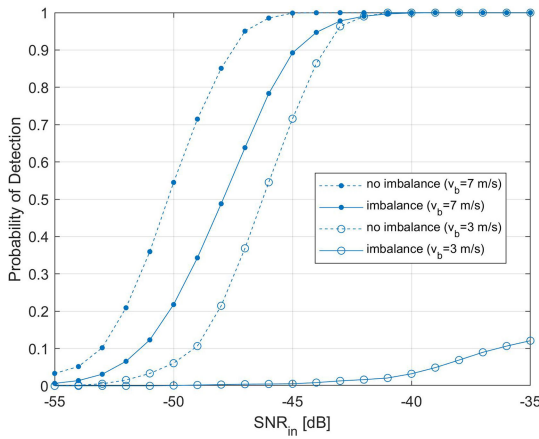


Fig. 7. PD as a function of target input SNR, for target bistatic velocities of 3 and 7 m/s, in the absence and in the presence of channel imbalance. Desired PFA is set to  $10^{-6}$ .

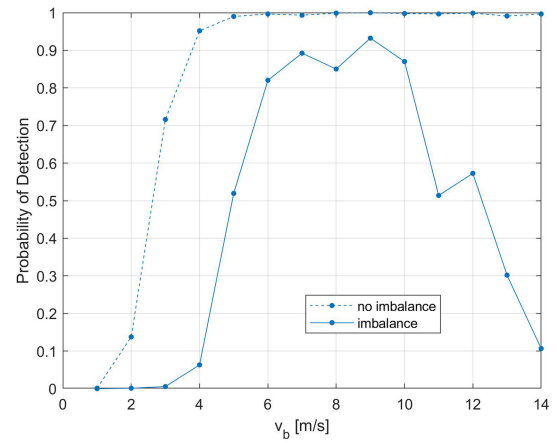


Fig. 8. PD as a function of target bistatic velocity, for target input SNR =  $-45$  dB, in the absence and in the presence of channel imbalance. Desired PFA is set to  $10^{-6}$ .

As a result, a Doppler-based calibration strategy would not be effective against target steering mismatches.

In this article, we propose two possible strategies for target detection, aimed at recovering the performance losses associated with channel calibration errors in a mobile passive radar exploiting a STAP scheme.

#### A. Spatially Noncoherent GLRT (NC-GLRT)

If the knowledge of channel imbalance in each desired steering direction is not possible, a simple potential solution can be to forgo a coherent integration in the spatial domain. If a small number of receiving channels are available, typically true in passive radar systems, this would produce a limited loss in terms of the final signal to disturbance ratio.

We propose a partially noncoherent space-time GLRT detector (referred to as NC-GLRT), where the steering vector is specified in the Doppler domain but not specified in the spatial domain, resulting in a noncoherent integration of the spatial target echoes.

Such a detector, first introduced in [14], can be derived along the line of the article presented in [37], where a polarimetric adaptive detection scheme is addressed. Considering the spatial component of the steering vector  $\mathbf{s}_s$  as a vector of unknown parameters, we replace it with its ML estimate during the derivation process. By defining the  $(NL \times N)$  matrix  $\mathbf{\Sigma} = \mathbf{s}_d \otimes \mathbf{I}_N$ , where  $\mathbf{I}_N$  is the  $N$ -dimensional identity matrix, the resulting GLRT detector is given by

$$\frac{\mathbf{x}^H \hat{\mathbf{Q}}^{-1} \mathbf{\Sigma} (\mathbf{\Sigma}^H \hat{\mathbf{Q}}^{-1} \mathbf{\Sigma})^{-1} \mathbf{\Sigma}^H \hat{\mathbf{Q}}^{-1} \mathbf{x}}{(1 + \mathbf{x}^H \hat{\mathbf{Q}}^{-1} \mathbf{x})} \geq \eta_2. \quad (6)$$

This detector keeps the CFAR property and the expression of the PFA follows (see [37]):

$$\text{PFA} = \frac{(1 - \eta_2)^{K-NL+1}}{(K - NL)!} \sum_{j=1}^N \frac{(K - NL + N - j)! \eta_2^{N-j}}{(N - j)!}. \quad (7)$$

This approach still performs an adaptive space-time filtering of data, aimed at whitening clutter returns. While, at

the expense of a limited loss in terms of maximum integration gain (and directivity), it is robust against losses due to spatial steering vector mismatches, thanks to a noncoherent integration of target echoes across the receiving channels.

### B. GLRT With Steering Vector Calibration (Cal-GLRT)

An alternative and more sophisticated approach consists of maintaining a fully coherent detection scheme and exploiting the information from stationary scene echoes to estimate the angle-dependent channel errors and define the correct spatial steering vector toward the desired target search direction.

The basic idea is to make use of the Doppler spread that characterizes clutter returns seen from a moving receiver and the corresponding relationship between the angle of arrival and Doppler frequency. In a similar fashion to the approaches in [13], Doppler frequency resolution can be exploited to isolate contributions from scatterers belonging to specific angular directions, thus allowing an estimation of the angle-dependent imbalance affecting the receiving channels. In this regard, the fine Doppler resolution provided by the typically long integration times of passive radar is an additional asset.

This principle has been exploited also in some previous works for array calibration in airborne radar [29]–[31], [33], [34]. The estimation of channel errors and the correct spatial steering vector in a specific direction can be made in different ways: for instance, by selecting principal eigenvector from clutter sample covariance matrix formed at the corresponding Doppler bin [30], [34]; or by least square estimation comparing returns of coregistered range-Doppler maps at the same Doppler bin [13], [33]. In this work, the latter approach is adopted.

Let us assume  $z^{(i)}[l, m]$  to be the complex value at generic range-Doppler bin of the range-compressed and Doppler-processed channel  $i$  after proper temporal coregistration. The imbalance estimated at the  $m$ th Doppler bin between channels  $i$  and  $j$  (assumed as reference) is given by

$$\hat{\Gamma}_{ij}[m] = \frac{\sum_{l=l_1}^{l_2} z^{(i)}[l, m] z^{(j)*}[l, m]}{\sum_{l=l_1}^{l_2} |z^{(j)}[l, m]|^2} \quad (8)$$

where the average is evaluated over consecutive range cells spanning indices from  $l_1$  to  $l_2$ .

The imbalance at the specific direction of interest  $\hat{\Gamma}_{ij}(\phi_0)$  can be obtained by selecting or interpolating the imbalance values estimated as a discrete function of Doppler bins in (8) at Doppler frequency  $f_D = v_p/\lambda \cos \phi_0$ .

Defining  $\Lambda(\phi_0) = \mathbf{I}_L \otimes \text{diag}\{[1, \hat{\Gamma}_{21}(\phi_0), \dots, \hat{\Gamma}_{N1}(\phi_0)]\}$ , the space-time coherent GLRT detector with calibrated steering vector (referred to as Cal-GLRT) is given by

$$\frac{|s^H \Lambda^H \hat{\mathbf{Q}}^{-1} \mathbf{x}|^2}{s^H \Lambda^H \hat{\mathbf{Q}}^{-1} \Lambda s \left(1 + \mathbf{x}^H \hat{\mathbf{Q}}^{-1} \mathbf{x}\right)} \gtrsim \eta_1. \quad (9)$$

At the expense of the additional cost required for steering vector calibration, this solution is expected to maximize the spatial integration gain on the target signal, provided that a good estimation of channel imbalance can be achieved. In addition, as we will show in the following, this scheme preserves phase information between the receiving channels, being suitable for target DoA estimation purpose.

## V. DETECTION OF PERFORMANCE ANALYSIS

In order to test and compare the performance of the proposed detection strategies, we consider the same simulated clutter scenario of Section III with  $N = 3$  receiving channels affected by the angle-dependent imbalance shown in Fig. 5. The ABPD-STAP approach is applied with  $L = 3$  Doppler bins and the number of training data is set to  $K = 54$ .

The detection performance is analyzed by means of Monte Carlo analyses for moving targets in the endoc clutter region. The NC-GLRT scheme in (6) and the Cal-GLRT scheme in (9) are compared with the standard GLRT detector in (4), where a mismatched steering vector is considered due to the channel imbalance. We refer to this latter case as mismatched GLRT. The case without imbalance is also considered as a reference.

Specifically, in Fig. 9(a), the results are shown in terms of estimated PD as a function of target input SNR for the same target parameters of Fig. 7. The desired PFA is set to  $10^{-6}$ .

As expected, both the solutions proposed in Section IV allow to mostly prevent the partial suppression of the target signal due to the channel imbalance and the resulting steering vector mismatch, largely recovering the detection performance losses. A significant difference in terms of minimum SNR required for a given PD can be noticed compared with the mismatched GLRT case (see solid blue curves), especially for lower target velocity. The performances of the ideal case (see blue dashed curves) are almost restored. Note that, although the considered solutions largely recover the performance losses caused by imbalance, the condition of perfectly balanced channels in all directions cannot be completely re-established.

The above considerations are also confirmed by looking at Fig. 9(b), where the PD is shown as a function of target bistatic velocity for a fixed SNR of  $-45$  dB. Both the proposed strategies allow a considerable reduction of target MDV by reducing the width of the clutter notch. The performance at higher velocity values is also considerably improved.

The Cal-GLRT detector (see green dash-dot curves) yields the best performance. In fact, the steering vector calibration allows to maximize the coherent integration gain of the target signal in the spatial domain.

Confirmation of the above can be found by looking at the target signal response at the output of the optimum filter, as shown in Fig. 10. As evident, a narrow clutter ridge is restored, thanks to the steering vector calibration. Small losses far from the clutter notch are still present (see depressions in Fig. 10) due to the mentioned dispersion of



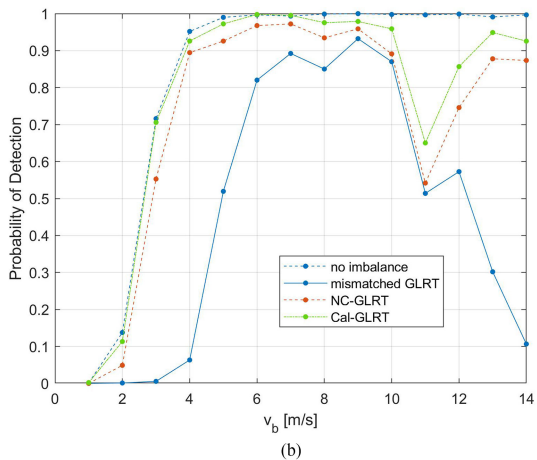
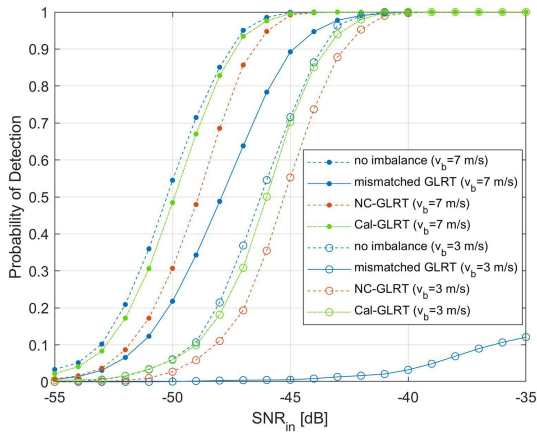


Fig. 9. Performance comparison of the considered detection schemes in the presence of channel imbalance. (a) PD as a function of target input SNR, for target bistatic velocities of 3 and 7 m/s. (b) PD as a function of target bistatic velocity, for target input SNR =  $-45$  dB. PFA is set to  $10^{-6}$ .

clutter energy in the angle-Doppler domain. They are mostly associated with sidelobe residual clutter contributions and depend on the specific angular behavior of the considered imbalance. They are responsible for the losses observable around 11 m/s in Fig. 9(b).

Notice that, in the considered simulated scenario, the homogeneous distribution of clutter facilitates the estimation of channel imbalance and the corresponding steering vector correction at the desired angular direction. In a real environment, strategies accounting for the potential variation of imbalance as a function of range or for the robustness of estimation against outliers, such as those described in [13], could be adopted.

The NC-GLRT approach (see red dashed curves in Fig. 9) only shows slight losses (in the order of 1–2 dB) compared with the Cal-GLRT case. These are mostly associated with a minor loss of noncoherent integration in the spatial domain (when using a small number of receiving channels). Nevertheless, it proves that an effective disturbance rejection capability is still preserved, despite the lower complexity due to the absence of an online calibration stage.

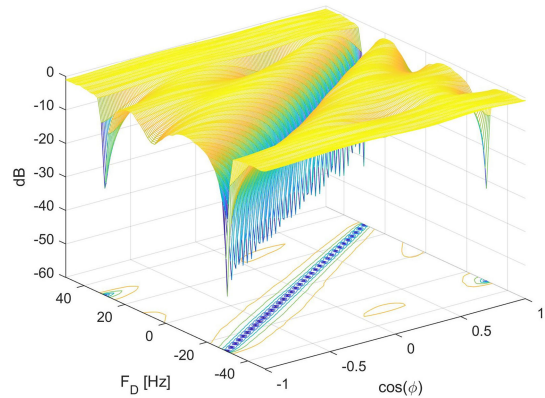


Fig. 10. Target signal response in the angle-Doppler domain at the output of the optimum space-time filter in the absence of noise and for known covariance matrix when considering the steering vector calibration.

Therefore, this last approach proves to be a suitable and simple solution for the purpose of target detection in mobile passive radar with few receiving channels, being robust against significant imbalance possibly affecting the channels.

## VI. TARGET DOA ESTIMATION

Typically, passive radar exploiting VHF/UHF bands are characterized by broad antenna beams and a limited number of array elements. Therefore, the accurate target localization represents a critical task and the interferometric approaches are commonly used to estimate the target DoA by exploiting the phase information across the available receiving channels.

Specifically, we refer to an ML DoA estimation approach for radar employing STAP (see [38]). Like the detection schemes in Section IV, DoA estimation can be performed after a nonadaptive transformation, aimed at containing the adaptivity losses and the required computational complexity.

By operating in the space-Doppler domain after the ABPD transformation of Fig. 2, the target angle estimate is obtained by maximizing the log-likelihood function with respect to  $\phi$

$$\hat{\phi}_t = \arg \max_{\phi} \left\{ \frac{|s^H(\phi) \hat{\mathbf{Q}}^{-1} \mathbf{x}|^2}{s^H(\phi) \hat{\mathbf{Q}}^{-1} \mathbf{s}(\phi)} \right\} \quad (10)$$

where unknown  $\phi_t$  represents the actual target DoA.

In practice, the ML estimate can be viewed as the location of the peak in a dense grid of adaptive matched filters [39]. Typically, the radar performs detection tests over a bank of filters coarsely spaced by the nominal beamwidth (BW) in angle. Once a target is detected, refined angle measurement is achieved through (10). The desired level of rms error is typically a one-tenth or one-twentieth of the BW.

The presence of an unknown imbalance affecting the receiving channels is a major problem for target detection

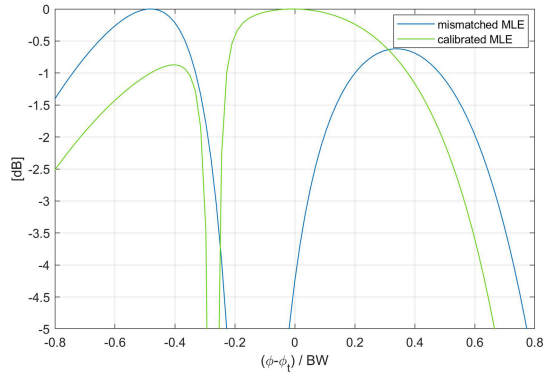


Fig. 11. Example of the likelihood functions of the ML DoA estimators in the known covariance matrix case when in the presence of channel imbalance. Target set at DoA  $85^\circ$  with bistatic velocity 3 m/s.

but even more for their accurate angular localization. An interchannel imbalance is expected to produce a significant degradation of DoA estimation accuracy. Although a non-coherent integration strategy in the spatial domain represents an effective solution for target detection, a coherent approach paired to a proper calibration of spatial steering vector is required when interested in target DoA estimation.

The same strategy, as adopted in Section III-B, for calibration of target steering vector based on returns from the stationary scene can be exploited to achieve a corrected ML DoA estimator.

By defining  $\mathbf{\Lambda}(\phi) = \mathbf{I}_L \otimes \text{diag}\{[1, \hat{\Gamma}_{21}(\phi), \dots, \hat{\Gamma}_{N1}(\phi)]\}$ ,  $\hat{\Gamma}_{ij}(\phi)$  being the estimated imbalance between channels  $i$  and  $j$  for each angle  $\phi$  in a dense grid around the direction of target detection, the ML DoA estimator with calibrated steering vector (referred to as calibrated MLE) is given by

$$\hat{\phi}_t = \arg \max_{\phi} \left\{ \frac{|s^H(\phi) \mathbf{\Lambda}^H(\phi) \hat{\mathbf{Q}}^{-1} \mathbf{x}|^2}{s^H(\phi) \mathbf{\Lambda}^H(\phi) \hat{\mathbf{Q}}^{-1} \mathbf{\Lambda}(\phi) s(\phi)} \right\}. \quad (11)$$

Imbalance  $\hat{\Gamma}_{ij}(\phi)$  for each test direction can be obtained by interpolating the imbalance estimated as a function of Doppler bins  $\hat{\Gamma}_{ij}[m]$  at Doppler frequency  $f_D = v_p/\lambda \cos \phi$ .

The DoA estimation accuracy of the standard ML estimator in (10), referred to as mismatched MLE, and of the calibrated version in (11) is evaluated by means of a Monte Carlo analysis against the same simulated clutter scenario of the previous sections. An ABPD-STAP approach is again applied with  $N = 3$  receiving channels, possibly affected by the angle-dependent imbalance shown in Fig. 5, and  $L = 3$  Doppler bins. The number of training data for disturbance covariance matrix estimation is set to  $K = 54$ . Both the estimators operate with a bank of filters equally spaced in angle by  $\delta\phi = 1^\circ$  within the nominal BW ( $\sim 57^\circ$ ) centered at  $\phi_0 = 90^\circ$ . The simulated target DoA is set to  $\phi_t = 85^\circ$ .

First, to appreciate the effect of a steering vector calibration on DoA estimation performance when in presence of channel imbalance, we show in Fig. 11 the likelihood function of (10) and (11) obtained in the known covariance

matrix case and in the absence of noise. Notice that the phase imbalance generates a bias error in the mismatched MLE case (blue curve), which is removed by the steering vector calibration (green curve). Moreover, especially for slower targets, also the width of the clutter notch plays a fundamental role.

In Fig. 12, the accuracy of the DoA estimators is compared as a function of target input SNR for bistatic velocities of 7 and 3 m/s. The results are shown in terms of standard deviation and bias of the estimation, both normalized to the nominal BW.

First, we notice that the presence of channel imbalance significantly degrades the accuracy of the mismatched MLE (see solid blue curves) by increasing both the standard deviation and the bias error, with respect to the case where no imbalance is present (see dashed blue curves). In particular, the resulting mismatch tends to polarize the DoA estimate, as clearly visible in Fig. 12(b), for high SNR values.

Conversely, it is evident that the calibrated MLE (see dash-dotted green curves) is able to mostly prevent the performance losses due to the channel imbalance, almost recovering the estimation accuracy of the ideal case.

To provide an additional reference for the DoA estimation accuracy of the considered scheme in the ideal case (namely in absence of imbalance) and to better evaluate the impact of channel errors and of the proposed calibration approach, we also consider the Cramér–Rao bound (CRB).

Following [40] and [41], and assuming known target Doppler frequency, the CRB after the nonadaptive ABPD transformation can be expressed as

$$\begin{aligned} \sigma_{\phi}^2 &= [\mathbf{J}^{-1}] \\ &= \left\{ 2|\bar{A}|^2 \left[ (\dot{s}^H(\phi) \mathbf{Q}^{-1} \dot{s}(\phi)) - \frac{|\dot{s}^H(\phi) \mathbf{Q}^{-1} s(\phi)|^2}{s^H(\phi) \mathbf{Q}^{-1} s(\phi)} \right] \right\}^{-1} \end{aligned} \quad (12)$$

where  $\sigma_{\phi}$  is the standard deviation of the DoA estimation error,  $\mathbf{J}$  is the Fisher information matrix,  $\bar{A}$  is the resulting target complex amplitude, and  $\dot{s}(\phi) = \partial s(\phi)/\partial \phi$ .

In Fig. 12(a), the corresponding CRB is reported for both the considered target velocities (solid and dotted gray curves). For high SNR values, there is a good match between the theoretical results and simulation. This is due to the ML nature of the estimator, which guarantees the condition of asymptotic efficiency. A little departure of the simulated results from the theory occurs for low SNR when the standard deviation of the estimate becomes comparable with the BW. This is, however, a case of limited interest. Also notice that, for higher SNR, the ML estimator is subjected to a saturation effect due to the use of a discrete set of angles (bank of filters) for DoA estimation.

## VII. EXPERIMENTAL RESULTS

In this section, the effectiveness of the proposed strategies for target detection and DoA estimation is demonstrated against a set of experimental data. The data are acquired by a multichannel passive radar mounted

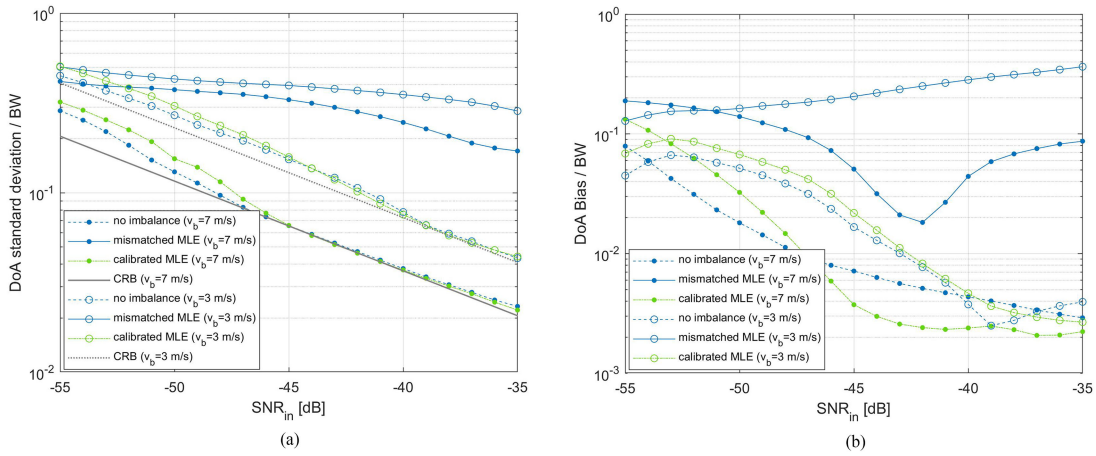


Fig. 12. Comparison of ML DoA estimation accuracy as a function of target input SNR. (a) Standard deviation normalized to BW. (b) Bias normalized to BW.



Fig. 13. Experimental multichannel receiver mounted on the back of a van in a side-looking configuration.

on a ground moving platform and based on DVB-T transmissions.

The acquisition campaign was carried out by Fraunhofer FHR in a rural area of the Eifel region in western Germany. The selected DVB-T illuminator of opportunity was the Eifel/Scharteberg transmitter. The radar system consisted of two Parasol units [41], each providing two receiving channels.

The four channels served as surveillance channels, while the reference signal is reconstructed from one of them. They were connected to discone antennas and displaced in the along-track direction. Radiation absorbing material was placed on one side to attenuate the backlobe contributions, thus forming a side-looking configuration. The system was mounted on a trailer behind a van (see Fig. 13). Table I summarizes the parameters of exploited DVB-T signal and the main acquisition and processing parameters.

The considered data scan is characterized by a bistatic geometry where the transmitter is located approximately in the direction opposite to the observed scene (see Fig. 14 for a sketch of the acquisition geometry). Moreover, an ultralight aircraft from Fraunhofer FHR (Delphin) has been employed as a cooperative target during the acquisition campaign.

The four receiving channels are affected by a considerable angle-dependent imbalance, as thoroughly described in

TABLE I  
Parameters of Experimental Test

Symbol	Description	Value
<b>DVB-T signal parameters</b>		
	DVB-T Standard	8k 16QAM
$f_c$	Carrier frequency	690 MHz
$N_c$	Number of useful carriers	6817
$T_u$	Useful symbol duration	896 us
$T_g$	Guard interval duration	224 us
$T_s$	OFDM symbol duration	1120 us
$B$	Bandwidth	7.61 MHz
<b>System and processing parameters</b>		
$v_p$	Platform velocity	$\sim 13.8$ m/s
$d_a$	Antenna spacing	0.36 m
$CPI$	Coherent processing interval	$512 T_s$

[13], where data from the same acquisition campaign were used. Differently from the DPCA case analyzed in [13], such imbalance is not expected to compromise the clutter suppression capability when an ABPD-STAP approach is adopted. However, it can have an impact on the moving target detection and localization performance, as described in the previous sections.

To prove the effectiveness of the proposed solutions in preventing the performance degradation due to steering vector mismatch, four simulated moving targets are injected into the real data, according to the model in (1), in addition to the real target Delphin. A proper imbalance is applied to the generated target echoes across the receiving channels, according to the imbalance estimated at the corresponding target DoA. The parameters of the real and the simulated targets are reported in Table II. Notice that the direction of the Delphin target is known only with a certain approximation.

Fig. 15 shows the range-Doppler maps resulting from the considered experimental dataset. Specifically, Fig. 15(a) represents the range-Doppler map obtained from a single channel, namely before STAP processing, scaled to the

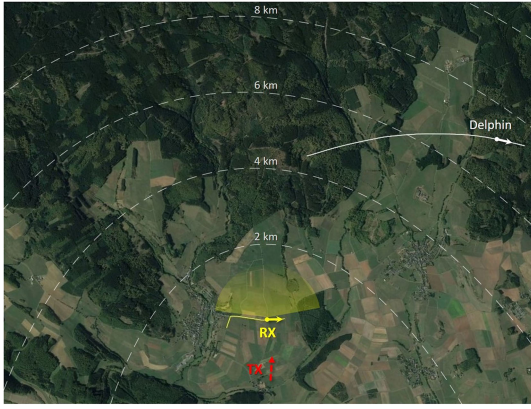


Fig. 14. Optical image showing the acquisition geometry. The receiver and aerial target position and direction of motion are indicated with yellow and white arrows, respectively. The red arrow indicates the transmitter's direction-of-arrival. Dashed lines represent the bistatic isorange curves.

TABLE II  
Target Parameters

Target	T1	T2	T3	T4	Delphin
$R_b$	4700 m	3700 m	6850 m	2500 m	6596 m
$v_b$	-6 m/s	6 m/s	11 m/s	4 m/s	-24.5 m/s
$\phi_t$	$37^\circ$	$157^\circ$	$109^\circ$	$70^\circ$	$\sim 37^\circ$
$SCNR_i$	-1 dB	-6 dB	-2 dB	-12 dB	2 dB
$SCNR_o$	17 dB	16 dB	12 dB	17 dB	15 dB

estimated noise power level. As evident, the clutter returns from the stationary scene extend over a Doppler bandwidth compatible with the platform velocity ( $v_p/\lambda \cong \pm 32$  Hz) and are characterized by a strong heterogeneity in terms of power levels across the map. Moreover, a strong direct signal contribution appears at the first bistatic range bin and low Doppler frequency, being the angle between the Rx–Tx line of sight and the platform velocity vector close to  $90^\circ$ .

The considered moving targets, due to their bistatic radial velocity and DoA, fall within the clutter Doppler bandwidth and appear as buried into clutter, being hardly detectable. Their positions are indicated by white boxes and their corresponding SCNR values are reported.

Fig. 15(b) shows the resulting range-Doppler map at the output of the space-time adaptive filter [numerator of (9)]. The ABPD-STAP scheme is applied with  $N = 4$  channels and  $L = 3$  Doppler bins. In this case, the number of training data is limited to  $K = 3NL = 36$  to account for the heterogeneity of the real clutter scenario. In fact, this can limit the number of available homogeneous secondary data, thus reducing the effectiveness of STAP.

The steering vector of the adaptive filter is selected toward the DoA of target T1 (i.e.,  $\phi_0 = 37^\circ$ ) and calibrated based on the imbalance estimated from clutter at the corresponding Doppler bin. With such steering, also the real target Delphin is expected to be included in the BW. For this reason, the SCNR values after STAP filtering are reported in the figure only for pointed targets T1 and Delphin. The other targets do not reach their maximum SCNR, since belonging

TABLE III  
Minimum Nominal PFA for Target Detection [ $\log_{10}(PFA)$ ]

	T1	T2	T3	T4	Delphin
<i>mismatched GLRT</i>	-1.4	-1.9	-3.4	-3.2	-1.8
<i>NC-GLRT</i>	-9.8	-13.7	-4.9	-8.3	-6.8
<i>Cal-GLRT</i>	-11.1	-15.3	-6.2	-9.7	-5.7
<i>Cal-GLRT @+5°</i>	-8.9	-14.7	-5.6	-9.4	-5.3
<i>Cal-GLRT @+10°</i>	-6.3	-13.5	-4.9	-5.2	-4.9

to different DoAs; however, they are still visible in the final map. The output SCNR values achievable when a proper steering vector is applied for each target are reported in Table II.

The above result clearly demonstrates the effective clutter suppression capability of the proposed STAP approach, which proves to be robust against the presence of angle-dependent calibration errors affecting the receiving channels.

To analyze more in detail the role of the solutions proposed in Section IV for target detection and to compare their performance, Fig. 16(a) and (b) reports the results obtained with the NC-GLRT detector in (6) and with the Cal-GLRT detector in (9), respectively.

Specifically, for each solution, we report the test statistics over the bistatic range-Doppler map before the application of a proper threshold, selected according to a desired value of nominal PFA. For a fair comparison, the test statistic is mapped into the PFA setting that would allow to exceed the corresponding threshold. In other words, each pixel in the map has been scaled so that it represents the minimum value of nominal PFA to be set for that pixel to yield a detection. Notice that the results are reported as  $\log_{10}(PFA)$ .

Target positions are indicated on maps by black boxes. Notice that, for the Cal-GLRT scheme in Fig. 16(b), the calibrated steering vector is again steered toward the DoA of targets T1 and Delphin. For this reason, the PFA values are compared in the figure only for the two targets belonging to the steering direction. For a complete comparison, in Table III, we report the minimum nominal PFA values to detect each target with the different detection schemes. Specifically, for the Cal-GLRT scheme, we consider the case where the selected direction for steering and calibration is coincident with each target DoA, and the cases where it deviates by  $5^\circ$  or  $10^\circ$  with respect to target angular positions, with targets still included in the nominal BW ( $\sim 23^\circ$ ). This is intended to simulate realistic detection conditions of a target search stage. Notice that such different target steering conditions are not considered for the NC-GLRT detector, which does not include a spatial steering vector component due to the noncoherent integration in the spatial domain. Finally, for comparison, the results obtained in the mismatched GLRT case are also reported.

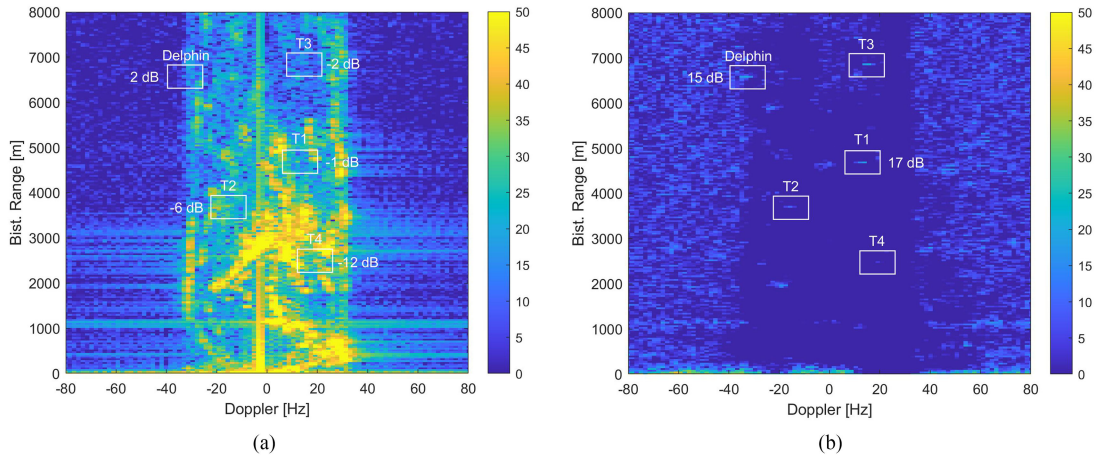


Fig. 15. Range-Doppler maps obtained from the experimental data. (a) Single-channel map. (b) Map after ABPD-STAP with calibrated steering vector toward the direction of targets  $T1$  and Delphin. Target positions are indicated by white boxes and the corresponding SCNR values are reported. SCNR after STAP filtering is reported only for targets belonging to the selected steering direction.

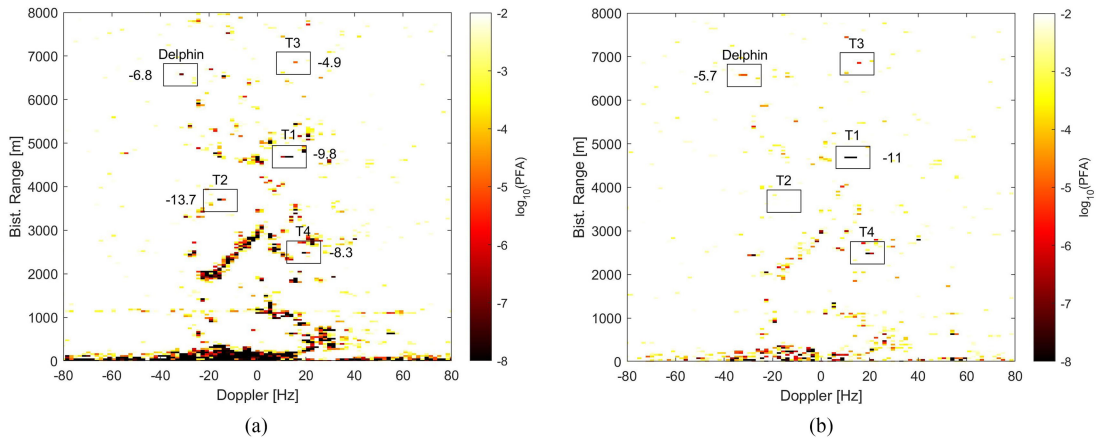


Fig. 16. Minimum nominal PFA to be set to detect each bin using (a) NC-GLRT scheme and (b) Cal-GLRT scheme with steering toward the direction of targets  $T1$  and Delphin. Values are expressed as  $\log_{10}(PFA)$ . Target positions are indicated by black boxes. PFA values for the Cal-GLRT case are reported only for targets belonging to the selected steering direction.

From the results in Fig. 16 and Table III, the following considerations are in order.

- The NC-GLRT scheme allows us to detect targets in all directions simultaneously (depending on the antenna element pattern), while the fully coherent scheme normally requires proper beam steering.
- The noncoherent integration yields a higher number of false alarms for the same PFA compared with the Cal-GLRT scheme, even at low PFA values, due to the enhancement of persistent clutter structures. However, notice that the NC-GLRT tends to integrate the false alarms accounting for all different angular directions.
- It is also worth noting that the presence of additional noncooperative moving targets in the scene during the acquisition cannot be excluded.
- The Cal-GLRT scheme yields better results with respect to the NC-GLRT when the steering is aligned with target DoA, allowing target detection until lower

values of PFA. The only exception is the Delphin target, where a slightly better result is achieved with the noncoherent approach. This is mostly because, for simulated targets, the imbalances were generated based on the clutter data; therefore, a perfect calibration can be reached with the adopted technique. While the real target, whose DoA may not exactly match the nominal one and which also features an elevation angle, may deviate from the imbalance estimated on the clutter.

- Accordingly, when the target DoA does not exactly coincide with steering direction (last two rows of Table III) but still falls within the BW and, therefore, detection is desirable, the NC-GLRT approach may outperform the Cal-GLRT also for the simulated targets. In this case, in fact, the estimated calibration may differ from that required by the target due to the angular variation of the channel imbalance. Nevertheless, both the considered solutions yield significantly better results compared with the mismatched GLRT case.

TABLE IV  
Target DoA Estimation Results

	T1	T2	T3	T4	Delphin
<i>mismatched MLE</i>	32.1° (-4.9°)	145.5° (-11.5°)	106.3° (-2.7°)	81.5° (+11.5°)	46.9° (+9.9°)
<i>calibrated MLE</i>	35.7° (-1.3°)	157.1° (+0.1°)	108.6° (-0.4°)	70.2° (+0.2°)	35.4° (-1.6°)

- Selecting a PFA of  $10^{-4}$ , all the considered targets would be detected by both the proposed detection approaches; conversely, none of them would be detected in the mismatched case.

In the coherent approach, the array nominal BW is in the order of  $23^\circ$ , thus offering poor target localization capability. An appropriate estimation of target DoA is then required.

To estimate the target angular position and verify the role of steering vector calibration in the target localization process, we consider the space-time ML DoA estimation approach proposed in Section VI. Specifically, it is applied for each target after the same ABPD transformation used for detection, exploiting the  $N = 4$  receiving channels,  $L = 3$  Doppler bins, and  $K = 36$  training data. A bank of filters equally spaced by  $\delta\phi = 0.1^\circ$  within the nominal BW is adopted.

The results of DoA estimation for each target are reported in Table IV for the mismatched MLE in (10) and the calibrated MLE in (11). The errors with respect to the corresponding true DoA values in Table II are reported in brackets.

It is evident that the steering vector calibration allows to significantly improve the estimation accuracy, preventing the negative impact of channel imbalance on the target localization performance. In fact, a correct DoA estimated is achieved for all targets, with an average error below one-thirtieth of the nominal BW. Notice that a slightly less accurate estimation is achieved for T1 and Delphin targets, whose DoA is far from the broadside direction.

The above results clearly demonstrate the effectiveness of the proposed strategies, both in terms of target detection and DoA estimation, in the presence of channel calibration errors.

From the above considerations, for a mobile passive radar equipped with a limited number of receiving channels, it seems reasonable to suggest the following operational strategy. A less demanding spatially noncoherent approach, such as in (6), which does not require an online calibration stage, could be adopted for the purpose of target detection. While an additional calibration stage could be applied in a fully coherent space-time scheme for DoA estimation, such as in (11), once the target has been detected.

## VIII. CONCLUSION

In this article, we addressed the problem of clutter rejection and slow-moving target detection and localization from a multichannel mobile passive radar in the presence of

antenna calibration errors. In particular, we considered the application of a post-Doppler STAP scheme and discussed the impact of channel calibration issues, proposing some practical solutions.

A newly conceived ABPD-STAP scheme was suggested as a suitable approach for mobile passive radar and its effectiveness was analyzed in terms of clutter cancelation and moving target detection against both simulated and real clutter scenarios. The new scheme is especially tailored to address the case of an angle-dependent imbalance affecting the receiving channels. In this case, the clutter cancelation capability is guaranteed by the adaptive degrees of freedom of the STAP filter. Nevertheless, we showed that the effects of target steering vector mismatch and of filter coefficients estimated for clutter suppression may result in gain losses and partial suppression of target signal at the output of the adaptive filter, as well as in inaccurate angular localization.

To address these points, the proposed ABPD-STAP scheme includes solutions aimed at recovering the target detection losses and performing an accurate DoA estimation.

i) First, to avoid large detection losses, we considered a detection scheme based on a spatially non-coherent space-time GLRT (NC-GLRT). With this approach, the steering vector is not specified in the spatial domain, resulting in a noncoherent integration of target echoes across the receiving channels. Our analysis showed that, at the expense of a limited loss in terms of maximum integration gain, this approach is robust against a significant imbalance affecting the received signal, preventing large detection losses. By entirely excluding the presence of a calibration stage, it represents a simple but effective solution for moving target detection, especially when few receiving channels are available.

ii) After a target detection stage based on the NC-GLRT, a calibrated space-time GLRT scheme (Cal-GLRT) is included to provide the target angular localization. In this scheme, the echoes from the stationary scene are exploited for an estimation of the angle-dependent channel errors and a proper correction of the spatial steering vector mismatch, making use of the clutter spread in Doppler and of the one-to-one relationship between the angle and Doppler frequency of stationary scatterers. This approach has been specifically devised for the case of passive radar STAP, where it is customary to operate with long coherent integration intervals and wide antenna beams, which allows the proposed calibration approach to operate effectively. In contrast, such an approach has not been considered for standard active radar STAP, where the typical narrow antenna beams and short integration times would limit the Doppler frequency resolution and, in turn, the angular resolution, thus restricting the ability to compensate for the imbalance variations. Our analysis showed that, at the expense of an additional calibration stage, the Cal-GLRT scheme could provide slightly better detection performance. Alternatively, it can be applied only to the potential targets detected by a first stage based on the NC-GLRT scheme to enable DoA estimation capability.

iii) Finally, we addressed the problem of target angular localization by DoA estimation, which represents a critical task in mobile passive radar featuring few wide beam antennas. We capitalized on the introduced steering vector calibration and assessed its key role in providing an accurate space time ML estimation of target DoA, by mitigating the negative impact of the unknown channel errors.

The effectiveness of the proposed solutions has been tested, in terms of moving target detection and localization, against both simulated and experimental data from a DVB-T-based multichannel mobile passive radar, showing an effective operation.

## REFERENCES

- [1] P. Lombardo and F. Colone  
Advanced processing methods for passive bistatic radar systems in *Principles of Modern Radar: Advanced Radar Techniques*, W. L. Melvin and J. A. Scheer, Eds. Hennigsdorf, Germany: SciTech, 2012, pp. 739–821.
- [2] J. Palmer, D. Cristallini, and H. Kuschel  
Opportunities and current drivers for passive radar research In *Proc. IEEE Radar Conf.*, 2015, pp. 145–150.
- [3] R. Klemm *et al.*, Eds. Novel radar techniques and applications in *Part III: Passive and Multistatic Radar*. London, U.K.: Inst. Eng. Technol., 2017.
- [4] L. M. H. Ulander, P. Frörlind, A. Gustavsson, R. Ragnarsson, and G. Stenström  
VHF/UHF bistatic and passive SAR ground imaging In *Proc. IEEE Radar Conf.*, 2015, pp. 0669–0673.
- [5] D. Gromek, K. Kulpa, and P. Samczyński  
Experimental results of passive SAR imaging using DVB-T illuminators of opportunity *IEEE Geosci. Remote Sens. Lett.*, vol. 13, no. 8, pp. 1124–1128, Aug. 2016.
- [6] K. Kulpa, M. Malanowski, and P. Samczyński  
Passive radar: From target detection to imaging In *Proc. IEEE Radar Conf.*, 2019, pp. 1–286.
- [7] Y. Fang *et al.*  
Improved passive SAR imaging with DVB-T transmissions *IEEE Trans. Geosci. Remote Sens.*, vol. 58, no. 7, pp. 5066–5076, Jul. 2020.
- [8] B. Dawidowicz, P. Samczynski, M. Malanowski, J. Misiurewicz, and K. S. Kulpa  
Detection of moving targets with multichannel airborne passive radar *IEEE Aerosp. Electron. Syst. Mag.*, vol. 27, no. 11, pp. 42–49, Nov. 2012.
- [9] B. Dawidowicz, K. Kulpa, M. Malanowski, J. Misiurewicz, P. Samczynski, and M. Smolarczyk  
DPCA detection of moving targets in airborne passive radar *IEEE Trans. Aerosp. Electron. Syst.*, vol. 48, no. 2, pp. 1347–1357, Apr. 2012.
- [10] P. Wojaczek, F. Colone, D. Cristallini, and P. Lombardo  
Reciprocal-filter-based STAP for passive radar on moving platforms *IEEE Trans. Aerosp. Electron. Syst.*, vol. 55, no. 2, pp. 967–988, Apr. 2019.
- [11] P. Wojaczek, D. Cristallini, and F. Colone  
Minimum variance power spectrum based calibration for improved clutter suppression in PCL on moving platforms In *Proc. IEEE Radar Conf.*, 2019, pp. 1–6.
- [12] G. P. Blasone, F. Colone, P. Lombardo, P. Wojaczek, and D. Cristallini  
A two-stage approach for direct signal and clutter cancellation in passive radar on moving platforms In *Proc. IEEE Radar Conf.*, 2019, pp. 1–6.
- [13] G. P. Blasone, F. Colone, P. Lombardo, P. Wojaczek, and D. Cristallini  
Passive radar DPCA schemes with adaptive channel calibration *IEEE Trans. Aerosp. Electron. Syst.*, vol. 56, no. 5, pp. 4014–4034, Oct. 2020.
- [14] G. P. Blasone, F. Colone, and P. Lombardo  
Facing channel calibration issues affecting passive radar DPCA and STAP for GMTI In *Proc. IEEE Int. Radar Conf.*, 2020, pp. 31–36.
- [15] X. Neyt *et al.*  
Feasibility of STAP for passive GSM-based radar In *Proc. IEEE Conf. Radar*, 2006, pp. 1–6.
- [16] J. Raout, X. Neyt, and P. Rischette  
Bistatic STAP using DVB-T illuminators of opportunity in *Proc. IET Int. Conf. Radar Syst.*, 2007, pp. 1–5.
- [17] P. Wojaczek, A. Summers, and D. Cristallini  
Preliminary experimental results of STAP for passive radar on a moving platform In *Proc. 22nd Int. Microw. Radar Conf.*, 2018, pp. 589–592.
- [18] Q. Wu, Y. D. Zhang, M. G. Amin, and B. Himed  
Space–time adaptive processing and motion parameter estimation in multistatic passive radar using sparse Bayesian learning *IEEE Trans. Geosci. Remote Sens.*, vol. 54, no. 2, pp. 944–957, Feb. 2016.
- [19] J. R. Lievsay and N. A. Goodman  
Modeling three-dimensional passive STAP with heterogeneous clutter and pulse diversity waveform effects *IEEE Trans. Aerosp. Electron. Syst.*, vol. 54, no. 2, pp. 861–872, Apr. 2018.
- [20] C. Berthillot, A. Santori, O. Rabaste, D. Poullin, and M. Lesturgie  
BEM reference signal estimation for an airborne passive radar antenna array *IEEE Trans. Aerosp. Electron. Syst.*, vol. 53, no. 6, pp. 2833–2845, Dec. 2017.
- [21] F. Wojaczek, D. Cristallini, J. Schell, and D. O’Hagan  
Polarimetric antenna diversity for improved reference signal estimation for airborne passive radar In *Proc. IEEE Radar Conf.*, pp. 1–6, Sep. 2020.
- [22] G. Chabriel and J. Barrère  
Adaptive target detection techniques for OFDM-based passive radar exploiting spatial diversity *IEEE Trans. Signal Process.*, vol. 65, no. 22, pp. 5873–5884, Nov. 2017.
- [23] V. Navrátil, A. O’Brien, J. L. Garry, and G. E. Smith  
Demonstration of space-time adaptive processing for DSI suppression in a passive radar In *Proc. Int. Radar Symp.*, 2017, pp. 1–10.
- [24] S. Gelli, A. Bacci, M. Martorella, and F. Berizzi  
Clutter suppression and high-resolution imaging of noncooperative ground targets for bistatic airborne radar *IEEE Trans. Aerosp. Electron. Syst.*, vol. 54, no. 2, pp. 932–949, Apr. 2018.
- [25] S. Searle, J. Palmer, L. Davis, D. W. O’Hagan, and M. Ummenhofer  
Evaluation of the ambiguity function for passive radar with OFDM transmissions In *Proc. IEEE Radar Conf.*, 2014, pp. 1040–1045.
- [26] G. Gassier, G. Chabriel, J. Barrère, F. Briolle, and C. Jauffret  
A unifying approach for disturbance cancellation and target detection in passive radar using OFDM *IEEE Trans. Signal Process.*, vol. 64, no. 22, pp. 5959–5971, Nov. 2016.
- [27] R. Klemm  
*Principles of Space-Time Adaptive Processing*, 3rd ed. London, U.K.: Inst. Eng. Technol., 2002.
- [28] J. R. Guerci  
*Space-Time Adaptive Processing for Radar*. Norwood, MA, USA: Artech House, 2003.
- [29] F. Le Chevalier, L. Savy, and F. Durniez  
Clutter calibration for space-time airborne MTI radars in *Proc. Int. Radar Conf.*, 1996, pp. 82–85.

- [30] M. A. Koerber and D. R. Fuhrmann  
Radar antenna calibration using range-doppler data  
In *Proc. IEEE 7th SP Workshop Statist. Signal Array Process.*, 1994, pp. 441–444.
- [31] F. C. Robey, D. R. Fuhrmann, and M. A. Koerber  
Array calibration and modelling of steering vectors  
In *Proc. Conf. Rec. 35th Asilomar Conf. Signals, Syst. Comput.*, 2001, pp. 1121–1126.
- [32] R. S. Blum and K. F. McDonald  
Analysis of STAP algorithms for cases with mismatched steering and clutter statistics  
*IEEE Trans. Signal Process.*, vol. 48, no. 2, pp. 301–310, Feb. 2000.
- [33] J. Ender  
The airborne experimental multi-channel SAR system AERII  
In *Proc. Eur. Synthetic Aperture Radar Conf.*, Mar. 1996, pp. 49–52.
- [34] C. H. Gierull  
Digital channel balancing of along-track interferometric SAR data  
Defence Res. Develop. Canada, Ottawa, ON, Canada, Tech. Rep. TM-2003-024, 2003.
- [35] J. Ward  
Space-time adaptive processing for airborne radar  
Lincoln Lab., Massachusetts Inst. Technol., Cambridge, MA, USA, Tech. Rep. 1015, 1994.
- [36] E. J. Kelly  
An adaptive detection algorithm  
*IEEE Trans. Aerosp. Electron. Syst.*, vol. AES-22, no. 2, pp. 115–127, Mar. 1986.
- [37] D. Pastina, P. Lombardo, and T. Bucciarelli  
Adaptive polarimetric target detection with coherent radar—Part I: Detection against Gaussian background  
*IEEE Trans. Aerosp. Electron. Syst.*, vol. 37, no. 4, pp. 1194–1206, Oct. 2001.
- [38] J. Ward  
Maximum likelihood angle and velocity estimation with space-time adaptive processing radar  
In *Proc. Conf. Rec. 30th Asilomar Conf. Signals, Syst. Comput.*, 1996, pp. 1265–1267.
- [39] F. C. Robey, D. R. Fuhrmann, E. J. Kelly, and R. Nitzberg  
A CFAR adaptive matched filter detector  
*IEEE Trans. Aerosp. Electron. Syst.*, vol. 28, no. 1, pp. 208–216, Jan. 1992.
- [40] R. Klemm  
Cramér-Rao analysis of reduced order STAP processors  
In *Proc. IEEE Int. Radar Conf.*, 2000, pp. 584–589.
- [41] F. Colone, D. Cristallini, D. Cerutti-Maori, and P. Lombardo  
Direction of arrival estimation performance comparison of dual cancelled channels space-time adaptive processing techniques  
*IET Radar, Sonar Navig.*, vol. 8, no. 1, pp. 17–26, Jan. 2014.
- [42] J. Heckenbach, H. Kuschel, J. Schell, and M. Ummerhofer  
Passive radar based control of wind turbine collision warning for air traffic PARASOL  
In *Proc. 16th Int. Radar Symp.*, 2015, pp. 36–41.



**Giovanni Paolo Blasone** (Student Member, IEEE) received the B.Sc. degree (*cum laude*) in electronic engineering, in 2012 and the M.Sc. degree (*cum laude*) in telecommunication engineering, in 2016 from the Sapienza University of Rome, Rome, Italy, where he is currently working toward the Ph.D. degree in radar and remote sensing with the Department of Information Engineering, Electronics, and Telecommunications.

He has been involved in research projects funded by the Italian Space Agency, the Italian Ministry of Research, and the radar industry. His main research interest focuses on the adaptive signal processing for multichannel radar systems and passive radar GMTI.

Mr. Blasone was a Finalist in the Student Paper Competition of the 2020 *IEEE International Radar Conference* in Washington, DC, USA, and in the 3MT contest of the 2020 *IEEE Radar Conference* in Florence, Italy.





**Fabiola Colone** (Senior Member, IEEE) received the B.Sc. and M.Sc. degrees in telecommunication engineering and the Ph.D. degree in remote sensing from the Sapienza University of Rome, Rome, Italy, in 2002 and 2006, respectively.

She joined as a Research Associate with DIET Department (formerly INFOCOM), Sapienza University of Rome, in January 2006. From December 2006 to June 2007, she was a Visiting Scientist with the Department of Electronic and Electrical Engineering, University College London, London, U.K. She is currently an Associate Professor with the Faculty of Information Engineering, Informatics, and Statistics, Sapienza University of Rome, Rome, Italy. The majority of her research activity is devoted to radar systems and signal processing. She has been involved, with scientific responsibility roles, in research projects funded by the European Commission, the European Defence Agency, the Italian Space Agency, the Italian Ministry of Research, and the radar industry. Her research has been reported in more than 140 publications in international technical journals, book chapters, and conference proceedings.

Dr. Colone has been a member of the Board of Governors of the IEEE Aerospace and Electronic System Society (AESS) since 2017, in which she is currently serving as a Vice-President for Member Services and an Editor in Chief for the IEEE AESS QEB Newsletters. Since 2019, she has been a member of the IEEE AESS Radar System Panel. She is also an Associate Editor for the IEEE TRANSACTIONS ON SIGNAL PROCESSING and a member of the Editorial Board of the *International Journal of Electronics and Communications* (Elsevier). She served the technical committee of many international conferences. She was in the organizing committee of the *IEEE 2008 Radar Conference* (Rome, Italy), as a Student Forum Co-Chair, and of the *IEEE 2020 Radar Conference* (Florence, Italy), as a Special Sessions Co-Chair. She is also a Technical Co-Chair of the *IEEE Radar Conference 2021* (Atlanta, USA). She was the co-recipient of the 2018 Premium Award for Best Paper in IET Radar, Sonar, and Navigation.



**Pierfrancesco Lombardo** (Senior Member, IEEE) received the Graduate degree in electronic engineering and the Ph.D. degree in remote sensing from the University of Rome “La Sapienza,” Rome, Italy, in 1991 and 1995, respectively.

After serving with the Official Test Centre of the Italian Air Force in 1992, he was an Associate with Birmingham University, U.K., and with Defence Research Agency in Malvern, in 1994. In 1995, he was a Research Associate with Syracuse University, Syracuse, NY, USA. In 1996, he joined the University of Rome “La Sapienza,” where he is currently a Full Professor. He is involved in, and coordinates, research projects funded by European and National Research Agencies and national industries. He leads the “Radar, Remote Sensing, and Navigation” group, University of Rome “La Sapienza.” He chairs the Cosmo-SkyMed consulting group for the Italian Space Agency. His main research interests include radar adaptive signal processing, radar clutter modeling, radar coherent detection, passive radar and multistatic radar, SAR processing, and radio-localization systems. His research has been reported in more than 280 publications in international technical journals and conferences and five book chapters.

Dr. Lombardo was a co-recipient of the Barry Carlton Award (Best Paper) of the IEEE TRANSACTIONS ON AEROSPACE AND ELECTRONIC SYSTEMS in 2001 and of the Best Paper Award for the IEEE TRANSACTION ON GEOSCIENCE AND REMOTE SENSING in 2003. He served the technical committee of many international conferences on radar systems and signal processing. He was a Technical Committee Chairman of the IEEE/ISPRS Workshop on Remote Sensing and Data Fusion over Urban Areas URBAN’2001, Rome, URBAN’2003, Berlin, and URBAN’2005, Tempe, USA, and also a Technical Chairman of the IEEE Radar Conference 2008. He is an Associate Editor for *Radar Systems* for the IEEE TRANSACTIONS ON AEROSPACE AND ELECTRONIC SYSTEMS (AES) since June 2001, and a Technical Editor for *Radar System* since January 2016. He is a member of the IEEE AES Radar System Panel and the Editorial Board of IET Proceedings on Radar, Sonar, and Navigation.



**Philipp Wojaczek** (Member, IEEE) received the M.Sc. degree in electrical engineering, electronics, and information technology from the Friedrich-Alexander-Universität Erlangen-Nürnberg, Erlangen, Germany, in 2014, and the Ph.D. degree in radar remote sensing from the University of Rome “La Sapienza,” Rome, Italy, in 2019.

Since 2015, he has been a Research Scientist with the Department for Passive Radar and Antijamming Techniques, Fraunhofer Institute for High Frequency Physics and Radar Techniques FHR, Wachtberg, Germany. His research interests include signal processing for passive radar systems and GMTI/SAR with airborne passive radar.

Dr. Wojaczek is a recipient of the Robert T. Hill Best Dissertation Award for his Ph.D. thesis awarded from the IEEE Aerospace and Electronic Systems Society (AESS) in 2019, and he coauthored the Best Poster Award at EUSAR 2018. Since 2020, he has been a Young Professional Representative for the IEEE AESS.



**Diego Cristallini** (Member, IEEE) was born in Terni, Italy, in 1981. He received the Graduate degree (*cum laude*) in telecommunication engineering and the Ph.D. degree in radar remote sensing with a thesis entitled “Innovative adaptive techniques for multichannel spaceborne SAR systems” from the University of Rome “La Sapienza,” Rome, Italy, in May 2006 and April 2010, respectively.

From December 2009 to February 2015, he was with the Department of Array-Based Radar Imaging, Fraunhofer Institute for High Frequency Physics and Radar Techniques FHR, Wachtberg, Germany. During this time, he has been working on the development of innovative space-time adaptive techniques for clutter suppression in multichannel airborne radar systems with special attention to bistatic systems and to highly nonhomogeneous clutter environments. Since March 2015, he has been leading the team on the passive covert radar with the Department of Passive Radar and Antijamming Techniques, Fraunhofer FHR, Germany. From March 2020 to June 2020, he was a Visiting Scientist with Defence Science and Technology (Group, Edinburgh, South Australia).

Dr. Cristallini is a co-chair of the NATO-SET 242 group on “PCL on moving platforms” and has been lecturing for the NATO LS-243 “Passive Radar Technology.” He was a recipient of the Best Paper Award at EUSAR 2014, co-authored the Best Poster Award at EUSAR 2018, and the co-recipient of the 2018 Premium Award for Best Paper in IET Radar, Sonar, and Navigation.